AGU PUBLICATIONS

JGR

Journal of Geophysical Research: Oceans

RESEARCH ARTICLE

10.1002/2016JC012048

Key Points:
- Vertical depth profiles of sinking particles were collected before the spring bloom
- Prebloom fluxes by small particles (<0.1 mm) were similar to bloom and postbloom export rates
- Small particles were likely exported by two mechanisms: aggregation/disaggregation and deep mixing

Supporting Information:
- Supporting Information S1

Correspondence to:
S. L. C. Giering,
s.giering@noc.ac.uk

Citation:
Giering, S. L. C., R. Sanders, A. P. Martin, C. Lindemann, K. O. Möller, C. J. Daniels, D. J. Mayor, and M. A. St. John (2016), High export via small particles before the onset of the North Atlantic spring bloom, *J. Geophys. Res. Oceans*, *121*, doi:10.1002/2016JC012048.

Received 11 JUN 2016
Accepted 17 AUG 2016
Accepted article online 19 AUG 2016

High export via small particles before the onset of the North Atlantic spring bloom

S. L. C. Giering[1], R. Sanders[1], A. P. Martin[1], C. Lindemann[2], K. O. Möller[3], C. J. Daniels[1,4], D. J. Mayor[1], and M. A. St. John[5]

[1]National Oceanography Centre, Southampton, UK, [2]Department of Biology, University of Bergen and Hjort Centre for Marine Ecosystem Dynamics, Bergen, Norway, [3]Institute for Hydrobiology and Fisheries Science, University of Hamburg, Hamburg, Germany, [4]Ocean and Earth Sciences, University of Southampton, Southampton, UK, [5]Section for Marine Ecology and Oceanography, Technical University of Denmark, Charlottenlund, Denmark

Abstract Sinking organic matter in the North Atlantic Ocean transfers 1–3 Gt carbon yr^{-1} from the surface ocean to the interior. The majority of this exported material is thought to be in form of large, rapidly sinking particles that aggregate during or after the spring phytoplankton bloom. However, recent work has suggested that intermittent water column stratification resulting in the termination of deep convection can isolate phytoplankton from the euphotic zone, leading to export of small particles. We present depth profiles of large (>0.1 mm equivalent spherical diameter, ESD) and small (<0.1 mm ESD) sinking particle concentrations and fluxes prior to the spring bloom at two contrasting sites in the North Atlantic (61.30°N, 11.00°W and 62.50°N, 02.30°W) derived from the Marine Snow Catcher and the Video Plankton Recorder. The downward flux of organic carbon via small particles ranged from 23 to 186 mg C m^{-2} d^{-1}, often constituting the bulk of the total particulate organic carbon flux. We propose that these rates were driven by two different mechanisms. In the Norwegian Basin, small sinking particles likely reached the upper mesopelagic by disaggregation of larger, faster sinking particles. In the Iceland Basin, a storm deepened the mixed layer to >300 m depth, leading to deep mixing of particles as deep as 600 m. Subsequent restratification could trap these particles at depth and lead to high particle fluxes at depth without the need for aggregation ("mixed-layer pump"). Overall, we suggest that prebloom fluxes to the mesopelagic are significant, and the role of small sinking particles requires careful consideration.

1. Introduction

The uptake of carbon dioxide by phytoplankton in the surface ocean and subsequent sinking of this organic matter to the ocean's interior—a process termed the "biological carbon pump"—plays an important role in controlling atmospheric carbon dioxide concentrations [*Falkowski et al.*, 1998]. Most of this sinking organic matter is thought to be carried by large aggregates (>0.5 mm [*Alldredge and Silver*, 1988]) composed of a mix of material including phytoplankton, detritus, inorganic matter, zooplankton moults, fecal material, and micro-organisms. This "marine snow" forms via physical coagulation and zooplankton-mediated aggregation [*Kiørboe*, 2001] predominantly in the upper ocean (mixed layer). Aggregates that sink below the mixed layer ("export") are rapidly consumed and reworked by the resident biota, thus forming the base of the mesopelagic food web [*Giering et al.*, 2014].

Particle formation via aggregation takes place most readily when phytoplankton concentrations are high [*Jackson*, 1990], for example, toward the end of a diatom bloom [*Burd and Jackson*, 2009]. In mid and high-latitude oceans, spring diatom blooms are a major feature of the annual cycle in plankton biomass and production. During the bloom phytoplankton reach a critical concentration at which aggregation occurs, leading to the formation and downward flux of aggregates [*Jackson*, 1990, 2005; *Kiørboe et al.*, 1994; *Jackson and Kiørboe*, 2008]. This leads to a strong seasonal cycle in the particle flux recorded by deep sediment traps [e.g., *Honjo and Manganini*, 1993; *Neuer et al.*, 1997; *Steinberg et al.*, 2001; *Lampitt et al.*, 2010]. In the North Atlantic, for example, long-term sediment trap deployments at 3000 m record strong peaks in particle flux around midsummer (approximately an order of magnitude higher than winter values), with the increase in flux at depth almost always following the increase in surface chlorophyll during spring [*Lampitt et al.*, 2010].

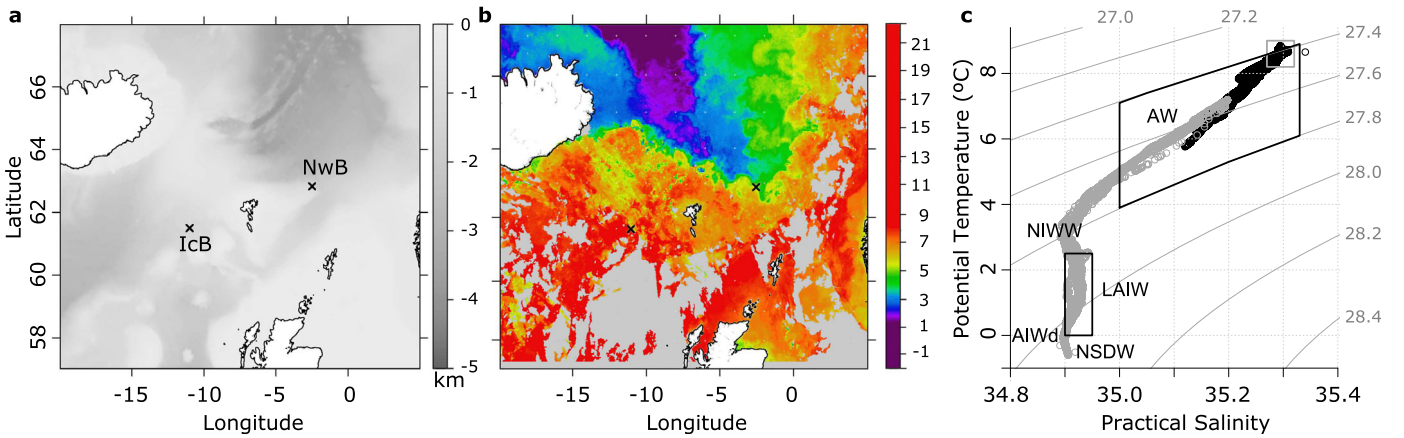

Figure 1. Details of the sampling area. (a) Sampling sites in the Iceland Basin ("IcB") and Norwegian Basin ("NwB") overlaid on the seabed topography. (b) Sea surface temperature between 30 January and 5 February 2012 (NEODAAS). (c) Salinity-temperature plots showing the different water masses in the IcB (black circles) and NwB (gray circles). Gray box identifies the upper 500 m in IcB. AW: Atlantic Water; NIWW: North Icelandic Winter Water; LAIW: Lower Arctic Intermediate Water; AIWd: deep Arctic Intermediate Water; NSDW: Norwegian Sea Deep Water.

Such observations suggest that prebloom deep flux rates are low and, when integrated, do not contribute significantly to total annual deep flux.

Conversely, *Körtzinger et al*. [2008] found that the highest deep flux (3000 m) at the Porcupine Abyssal Plain site in the North Atlantic coincided with the onset of water column stratification. A similar observation was made in the Norwegian Sea based on Bio-Argo float backscattering profiles; calculated export fluxes from the euphotic zone by small (approximately 0.2–20 μm) particles were highest at the time of mixed-layer shoaling [*Dall'Olmo and Mork*, 2014].

In this study we investigate the hypothesis that significant export occurs before the spring bloom in the North Atlantic. Depth profiles of particles were investigated over 7 weeks using the Marine Snow Catcher (MSC) and the Video Plankton Recorder (VPR) at two contrasting sites. We discuss how a storm affected stratification and chlorophyll distributions, and what may have controlled prebloom particle fluxes.

2. Methods

2.1. Site Description

Particles were photographed using the VPR and collected with the MSC between 19 March and 2 May 2012 at two open ocean sites in the high-latitude North Atlantic during FS *Meteor* cruise M87/1 (Figures 1a and 1b). The aim of the cruise was to investigate the mechanisms leading to the development of the spring bloom. Station 1 ("IcB") was located south of the Iceland-Faroe Ridge (61.30°N, 11.00°W) in the Iceland Basin and was occupied four times during the cruise (25–28 March, 7–11 April, 18–21 April, and 27–30 April). Station 2 ("NwB") was located north of the ridge in the southern part of the Norwegian Sea (62.50°N, 02.30°W) and was occupied three times (30 March–1 April, 12–14 April, and 22–25 April). At each station, depth profiles of temperature, salinity, and fluorescence were recorded using vertical CTD casts. CTD fluorescence was calibrated against Chlorophyll a (Chl) measurements made on 90% acetone extracts (24 h, 4°C) from samples collected in the upper 115 m of the water column ($P < 0.001$, $R^2 = 0.76$, $n = 75$). The mixed-layer depth (MLD) was defined as the depth at which the potential density, σ_Θ, was >0.05 kg m^{-3} higher than the surface density ($\Delta\sigma_\Theta$) [*Brainerd and Gregg*, 1995]. An alternative method defines the mixed layer as the depth at which the temperature is >0.5°C higher than sea surface temperature. Both methods agreed well. The mixing layer was determined using $\Delta\sigma_\Theta$ of 0.005 kg m^{-3} [*Brainerd and Gregg*, 1995]. The buoy "K5" (Met Office) located 270 km south of IcB provided data on average wind speed and dominant wave height.

2.2. Particle Collection

Suspended and sinking particles were sampled at four depths between 50 and 650 m during each visit in the IcB and NwB using the MSC (Figure 2a). The MSC was successfully deployed 27 times during the cruise at the

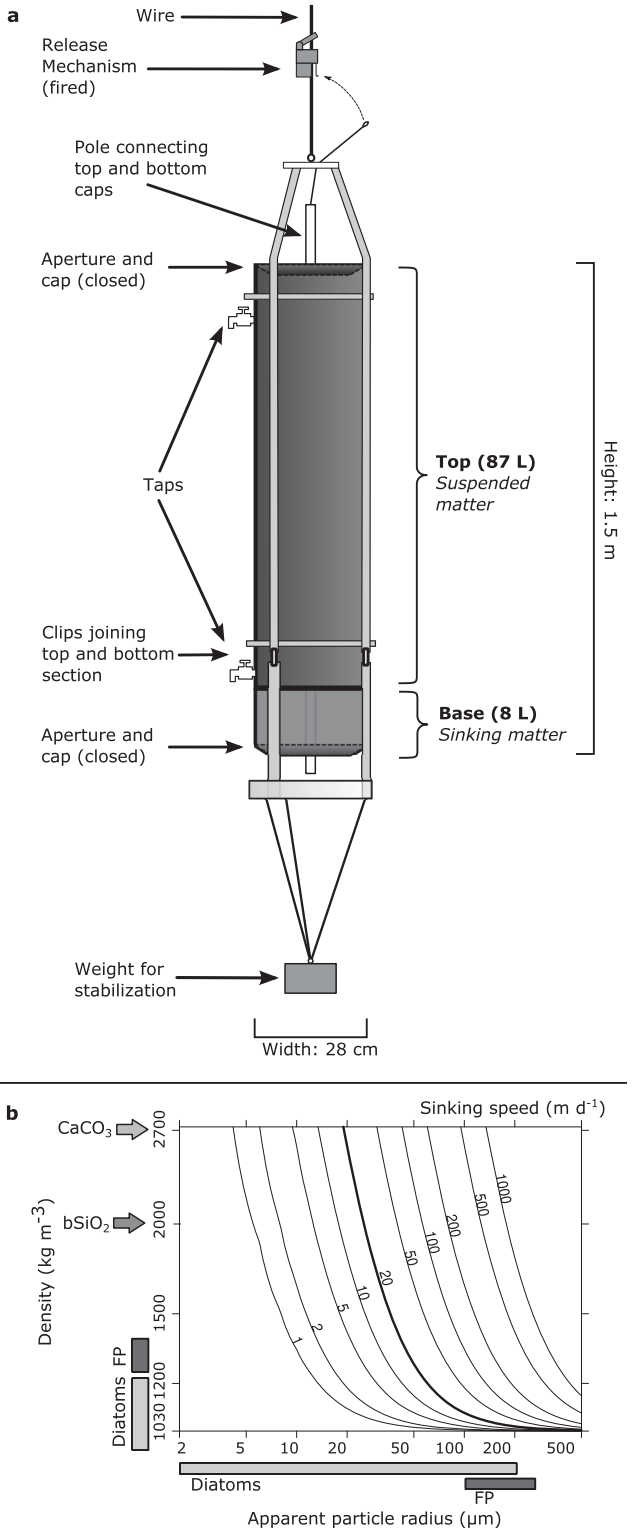

Figure 2. (a) Schematic of the Marine Snow Catcher. (b) Sinking speed (m d^{-1}) as function of particle radius (μm) and density (kg m^{-3}) calculated using Stoke's law. Density and viscosity of seawater was as observed in the IcB. Gray bars show ranges observed for diatoms [*Van Ierland and Peperzak*, 1984] and copepod fecal pellets (FP) [*Frangoulis et al*., 2001; *Komar et al*., 1981]. Arrows indicate density of $CaCO_3$ and $bSiO_2$. Sinking speed assumed for fluxes in the MSC (~20 m d^{-1}) is highlighted.

two sites, providing seven depth profiles between 50 and 650 m. Details of the deployments are listed in Table 1.

For a full description of the MSC and how it can be used to estimate particle fluxes, see *Riley et al*. [2012]. It has been used to measure particle fluxes in the North Atlantic [*Riley et al*., 2012; A. Belcher et al., Depth-resolved particle associated microbial respiration in the northeast Atlantic, submitted to *Biogeosciences Discussion*, 2016] and in the Southern Ocean [*Cavan et al*., 2015; *Belcher et al*., 2016]. In brief, the MSC is a large volume (95 L) water sampler with a removable base section that holds 8 L. During deployment, the two sections of the MSC are attached and the terminal apertures of the sampler are open allowing water transport through the sampler with minimal turbulence. Upon arrival at the desired depth, a trigger is released and the apertures are closed. After recovery of the device, 5 L are decanted from the top section as "time zero" (t_0). The MSC is subsequently secured on deck and particles left to settle for 2 h. The top section of the MSC is then drained slowly (2–3 L min^{-1}) through the bottom tap to minimize resuspension of settled particles. To estimate the concentration of suspended material (here operationally defined as matter still remaining in the top section after the settling period), the drained water is subsampled at the beginning and the end of draining procedure. The top section of the MSC is then removed. All visible aggregates ("large" particles with a diameter of >0.1 mm) are removed from the bottom of the base section using a pipette. The remaining water in the base section is subsampled to estimate the concentration of small (<0.1 mm) sinking particles. All water samples were analyzed for particulate organic carbon (POC), particulate organic nitrogen (PON), particulate inorganic carbon ($CaCO_3$), and biogenic silica ($bSiO_2$).

Large particles were photographed using a microscope camera (Motic

Journal of Geophysical Research: Oceans

10.1002/2016JC012048

Table 1. Concentrations and Fluxes of POC, PON, $CaCO_3$, and $bSiO_2$ in the Suspended and Small Sinking Particle Fractions in the Iceland Basin (IcB) and Norwegian Basin (NwB) as Measured Using the MSC[a]

				Concentrations ($\mu g\ L^{-1}$)																Fluxes ($mg\ m^{-2}\ d^{-1}$)									
				Suspended								Small Sinking								Small Particles								Large Particles	
Station	Visit	Date	Depth (m)	POC	S.D.	PON	S.D.	$CaCO_3$	S.D.	$bSiO_2$	S.D.	POC	S.D.	PON	S.D.	$CaCO_3$	S.D.	$bSiO_2$	S.D.	POC	S.D.	PON	S.D.	$CaCO_3$	S.D.	$bSiO_2$	S.D.	POC	S.D.
IcB	1	28 Mar 12	50	84.2	2.3	6.5	0.7	8.2	0.8	6.9	0.5	9.8	0.4	0.5	0.1	1.1	0.1	0.1	0.1	185.8	7.8	10.1	1.8	20.4	1.5	2.5	1.0	0.0	
IcB	1	25 Mar 12	175	114.4	23.4	2.4	0.9	4.1	0.1	2.2	0.3	1.6	2.0	0.3	0.1	0.6	0.0	1.4	0.1	30.5	37.5	6.4	2.0	12.0	0.5	26.8	1.2	0.0	
IcB	1	27 Mar 12	200	80.2	4.2	0.4	0.6	5.8	0.2	7.5	0.3	6.8	0.4	0.5	0.1	1.5	0.1	0.1	0.0	128.6	8.3	9.8	1.7	28.4	1.1	1.3	0.7	0.0	
IcB	1	26 Mar 12	650	111.9	9.3	6.1	0.7	8.9	0.7	4.6	0.3	NA	NA	NA	NA	0.5	0.1	0.0	0.0	69.1	73.2	3.9	4.1	9.7	1.1	0.7	0.7	0.0	
IcB	2	09 Apr 12	200	73.4	2.7	3.5	0.7	6.0	0.4	14.1	0.3	5.7	0.3	0.9	0.1	0.5	0.0	0.1	0.0	107.6	6.0	17.0	1.8	9.6	0.8	1.4	0.7	0.8	0.1
IcB	2	10 Apr 12	200	89.6	2.4	5.4	0.6	4.7	0.2	8.0	0.4	2.8	0.2	0.2	0.1	0.1	0.0	0.2	0.0	52.7	4.5	2.9	1.7	2.6	0.3	3.6	0.9	0.0	0.0
IcB	2	10 Apr 12	400	78.8	0.6	5.0	0.6	4.2	0.1	8.3	0.7	1.9	0.1	0.2	0.1	0.3	0.0	−0.4	0.1	35.4	2.0	4.0	1.7	4.8	0.3	−6.7	1.3	0.5	0.1
IcB	2	10 Apr 12	550	57.6	1.9	0.6	0.7	4.5	0.2	3.9	0.3	2.6	0.2	0.1	0.1	0.3	0.0	0.1	0.0	50.2	3.7	2.3	1.8	6.0	0.4	1.9	0.7	2.8	0.5
IcB	3	21 Apr 12	50	78.2	3.9	10.4	0.8	10.6	0.1	33.1	0.3	5.4	0.4	0.9	0.1	0.4	0.0	1.3	0.1	101.9	7.4	17.4	2.0	6.8	0.4	25.0	1.2	16.8	4.7
IcB	3	21 Apr 12	200	63.4	4.1	5.3	0.6	9.3	0.4	19.9	0.3	NA	NA	NA	NA	0.3	0.0	1.3	0.1	56.3	9.2	5.7	0.9	5.2	0.7	24.4	1.1	5.4	1.3
IcB	3	20 Apr 12	400	23.2	0.6	1.1	0.6	6.1	0.5	12.0	1.1	3.4	0.1	0.5	0.1	NA	NA	0.4	0.1	65.5	2.8	8.8	1.7	NA	NA	6.9	1.9	3.9	0.9
IcB	3	19 Apr 12	600	60.2	2.6	3.3	0.8	9.5	0.1	17.3	0.5	2.1	0.2	0.3	0.1	0.3	0.0	0.7	0.1	40.2	4.6	5.5	1.9	6.3	0.4	12.7	1.1	47.4	5.0
IcB	4	29 Apr 12	50	80.3	1.1	11.1	0.9	8.4	0.4	43.2	0.8	4.3	0.2	0.7	0.1	0.3	0.0	2.2	0.1	81.3	3.6	13.1	2.1	4.8	0.7	41.0	2.1		
IcB	4	29 Apr 12	120	58.4	4.4	6.6	0.9	9.8	0.4	45.5	0.6	NA	NA	NA	NA	0.3	0.0	1.2	0.1	23.4	4.0	2.9	0.5	5.4	0.8	22.3	1.4		
IcB	4	28 Apr 12	200	77.6	0.6	11.5	0.6	8.1	0.4	39.0	1.3	4.2	0.2	0.9	0.1	0.5	0.0	1.3	0.1	79.9	3.2	17.0	1.8	9.2	0.8	25.6	2.3		
IcB	4	28 Apr 12	400	64.8	1.8	8.0	0.7	7.8	0.4	33.7	2.1	NA	NA	NA	NA	0.2	0.0	0.9	0.2	25.8	8.8	3.1	1.0	2.9	0.6	16.7	3.4		
IcB	4	27 Apr 12	600	70.9	0.6	6.1	0.6	8.8	1.4	12.6	2.4	6.2	0.2	0.2	0.1	0.1	0.1	0.6	0.2	117.8	4.5	4.2	1.7	2.6	2.3	10.6	3.9		
			Average	74.5		5.5		7.3		18.3		4.4		0.5		0.4		0.7		73.7		7.9		8.5		12.8		6.5	
			SD	21.0		3.4		2.2		14.7		2.4		0.3		0.4		0.7		43.5		5.3		6.9		12.9		13.8	
NwB	1	30 Mar 12	200	97.2	9.3	3.0	0.8	9.6	0.5	7.3	0.3	4.0	0.8	0.5	0.1	0.3	0.0	0.4	0.0	76.6	15.2	9.8	1.9	4.8	0.8	8.1	0.8	0.0	
NwB	1	31 Mar 12	200	107.0	0.8	4.8	0.6	7.1	0.2	4.0	0.9	1.5	0.1	0.4	0.1	0.9	0.0	0.8	0.1	29.2	2.1	8.5	1.7	17.4	0.8	14.6	1.6	0.0	
NwB	2	14 Apr 12	50	82.4	0.6	10.7	0.7	11.6	0.4	11.5	1.2	1.3	0.1	0.3	0.1	0.1	0.0	0.0	0.1	25.6	1.8	6.2	1.7	2.3	0.7	0.0	1.9	9.7	2.8
NwB	2	13 Apr 12	100	89.4	2.1	5.1	0.7	10.1	0.6	8.6	0.4	4.8	0.3	0.6	0.1	0.1	0.1	−0.1	0.0	90.5	4.9	12.2	1.8	1.9	1.0	−1.9	0.9	2.7	0.3
NwB	2	13 Apr 12	250	113.8	0.7	10.3	0.7	10.3	0.4	9.4	0.3	5.1	0.2	1.2	0.1	0.2	0.0	0.3	0.0	96.8	3.9	22.9	1.9	4.4	0.7	4.8	0.8	2.9	0.4
NwB	2	14 Apr 12	600	63.2	0.6	1.6	0.6	8.1	0.1	6.0	0.4	2.0	0.1	0.4	0.1	0.0	0.0	0.4	0.0	38.8	2.1	6.9	1.7	0.8	0.3	7.4	0.9		
NwB	3	25 Apr 12	50	110.0	3.7	15.9	0.9	22.1	0.1	13.8	0.3	4.7	0.4	0.7	0.1	0.9	0.0	0.1	0.0	88.5	6.9	13.8	2.1	16.7	0.7	1.9	0.7	18.4	1.8
NwB	3	25 Apr 12	120	50.0	5.4	4.7	1.2	13.8	0.5	10.8	0.3	6.8	0.5	0.7	0.1	1.1	0.1	1.3	0.1	129.5	9.9	13.0	2.3	21.6	1.2	24.8	1.2	2.1	0.7
NwB	3	23 Apr 12	250	35.4	1.2	2.7	0.8	7.3	0.3	7.2	0.3	4.4	0.2	0.5	0.1	0.4	0.0	0.3	0.0	83.1	3.8	10.0	1.9	6.9	0.6	4.9	0.7	2.0	0.3
NwB	3	23 Apr 12	600	43.4	0.6	3.5	0.6	7.2	0.6	7.1	1.1	2.2	0.1	0.4	0.1	0.2	0.0	0.5	0.1	42.0	2.1	8.1	1.7	3.9	0.9	10.0	1.8	0.1	0.0
			Average	79.2		6.2		10.7		8.6		3.7		0.6		0.4		0.4		70.1		11.2		8.1		7.5		4.2	
			SD	29.2		4.6		4.5		2.9		1.8		0.3		0.4		0.4		34.4		4.9		7.5		7.8		6.1	

[a]Large particle fluxes were calculated from particle numbers, measured sinking speed, and estimated particle carbon content.

Moticam 1000 CMOS 1/2″, 1.3 mega pixels, 1280 × 1024). Particle photos were analyzed using ImageJ (v1.49 [*Schindelin et al*., 2012]), particles counted, and for each particle volume and equivalent spherical diameter (ESD) were calculated assuming fecal pellets were cylindrical and all other particles were prolate ellipsoids. POC content of large sinking particles was calculated following *Alldredge* [1998]: POC (μg) = 0.99 × $V^{0.52}$, where V is the particle volume (mm^3). Unfortunately, no photos were taken from deployments on the 27–29 April.

The sinking speeds of up to 20 particles from each MSC deployment (total n = 132) were measured in the controlled-temperature laboratory (at ambient sea surface temperature) using a 1 L measuring cylinder filled with water from the suspended fraction of the respective MSC deployment. Using a pipette, individual particles were carefully transferred approximately 5 cm below the water surface, and sinking speed was recorded three times over a total distance of 7.5 cm (median R.S.D. = 0.09, n = 132).

2.3. Sample Analyses

Concentrations of POC and PON were determined by filtering 1000 mL seawater onto precombusted (450°C, 12 h) GF/F filters (25 mm diameter, Whatman). Filters were dried (40°C, 24 h) and stored for subsequent analysis. On shore, filters were fumed with concentrated sulfurous acid for 24 h, dried (60°C, 24 h) and pelleted in tin cups (Elemental microanalysis). POC and PON were analyzed from the same filter using an ANCA NT prep system coupled with a 20-20 Stable Isotope Analyser (PDZ Europa Scientific Instruments, Northwich, UK) as described by *Flynn and Davidson* [1993]. Calibration was performed using a solution of isoleucine (L-Isoleucine, Sigma) at concentrations of 1 μg N and 5.14 μg C, and with series of standards from 5.34 to 106.8 μg N and 27.44 to 548.95 μg C at the beginning of each batch. Reference samples were analyzed after every eight samples to check the instrument precision, and a drift correction was applied. All samples were blank corrected. Twenty-six of the 95 PON samples were below the calibration range, 18 of these gave values below the detection limit (3 × S.D. of blank: 3.75 μg N). We included all PON samples for the calculation of fluxes as the uncertainty in these low concentration estimates will not alter the overall interpretation, but we acknowledge that the resulting small PON fluxes need to be viewed with caution especially when calculating C:N ratios. POC and PON were assumed to have a molecular mass of 12 and 14, respectively.

Concentrations of $CaCO_3$ were determined following *Daniels et al*. [2015] by filtering 500 mL onto 0.8 μm polycarbonate filters, rinsing them with pH-adjusted (pH 9, using ammonium hydroxide) MilliQ water. Filters were dried (40°C, 24 h) and stored until later analysis. On shore, samples were digested for 24 h using 20 mL HNO_3 (0.4 *M*), and filtered through a PTFE syringe filter (0.45 μm pore size, 25 mm diameter, Whatman). Samples were analyzed using an ICP-OES measuring sodium (589.6 nm) and calcium at three different wavelengths (315.9, 317.9, and 422.7 nm). Results were corrected for sea salt, which was negligible in this case. $CaCO_3$ was assumed to have a molecular mass of 100. $bSiO_2$ was determined following *Brown et al*. [2003] by filtering 500 mL onto 0.8 μm polycarbonate filters which were then dried (40°C, 24 h) and stored until later analysis. On shore, filters were digested using 0.2 *M* NaOH (80°C, 4 h), neutralized with 0.1 *M* HCl, and silicate concentrations determined using a Skalar SanPlus autoanalyser. $bSiO_2$ was assumed to have a molecular mass of 60.

2.4. Calculation of Concentrations and Fluxes

Concentrations of suspended, small (<0.1 mm ESD) and large (>0.1 mm ESD) sinking particles were calculated based on *Riley et al*. [2012]. During the settling period some of the organic matter sinks, causing increased concentrations in the base section compared to the top section. The difference in the concentrations between the two sections was used to calculate the concentration of suspended sinking matter (p_{sus}; μg L^{-1}) and small sinking matter (p_{small}; μg L^{-1}):

$$p_{sus} = p_{top}, \tag{1}$$

$$p_{small} = (p_{base} - p_{top}) \times V_{base}/V_{MSC}, \tag{2}$$

where p_{top} and p_{base} are, respectively, the concentrations (μg L^{-1}) in the top section (average of the two samples taken from the top section during draining) and base section, and V_{base} and V_{MSC} are the volume of the base section (8 L) and the MSC (95 L incl. base), respectively. Fluxes of small sinking particles (F_{small};

μg m^{-2} d^{-1}) were calculated from p_{small} divided by the area of the MSC base (A_{MSC}; 0.06 m^2) and the settling time (t; 2 h)

$$F_{small} = p_{small} \times V_{MSC} \times (A_{MSC} \times t)^{-1}. \quad (3)$$

POC and PON samples for the base section of four MSC were lost during analysis. Fluxes for these depths were estimated using $CaCO_3$ and $bSiO_2$ fluxes multiplied by the average C:$CaCO_3$ and C:$bSiO_2$ ratios of all samples taken from the respective MSC deployment. This method, when applied to MSC data where the base sample was present, underestimated MSC-derived fluxes in 87% of the cases.

The assumed average sinking velocity of small particles is determined by the height of the MSC (1.5 m) and the settling time (2 h), and is 18 m d^{-1}. This rate is in broad agreement with the sinking speeds of small spherical particles calculated from the density difference between the particle and the ambient water following Stoke's law (Figure 2b). Particles such as single diatom cells, small phytoplankton aggregates, and small fecal pellets, are likely to sink at 0–150 m d^{-1} (Figure 2b), consistent with measured sinking rates of phytoplankton of diverse taxonomic composition (0.32–1.69 m d^{-1} [*Bienfang*, 1981]) and of small (<0.5 mm length) fecal pellets (5–153 m d^{-1} [*Turner*, 2002]). The fluxes of small particles we calculate represent lower limits of the true flux. This is because the concentration gradient between the top and the bottom section of the MSC (equation (2)) established sometime during the settling period of 2 h. Reducing the time term in equation (3) from 2 h to a shorter time period leads to an increase in calculated fluxes; thus, the presented fluxes are lower limits.

The flux of large sinking particles (F_{large}; μg m^{-2} d^{-1}) was calculated using a derivation of equation (3)

$$F_{large} = \sum (m_{particle} \times v_{particle} \times h^{-1}) \times A_{MSC}{}^{-1}. \quad (4)$$

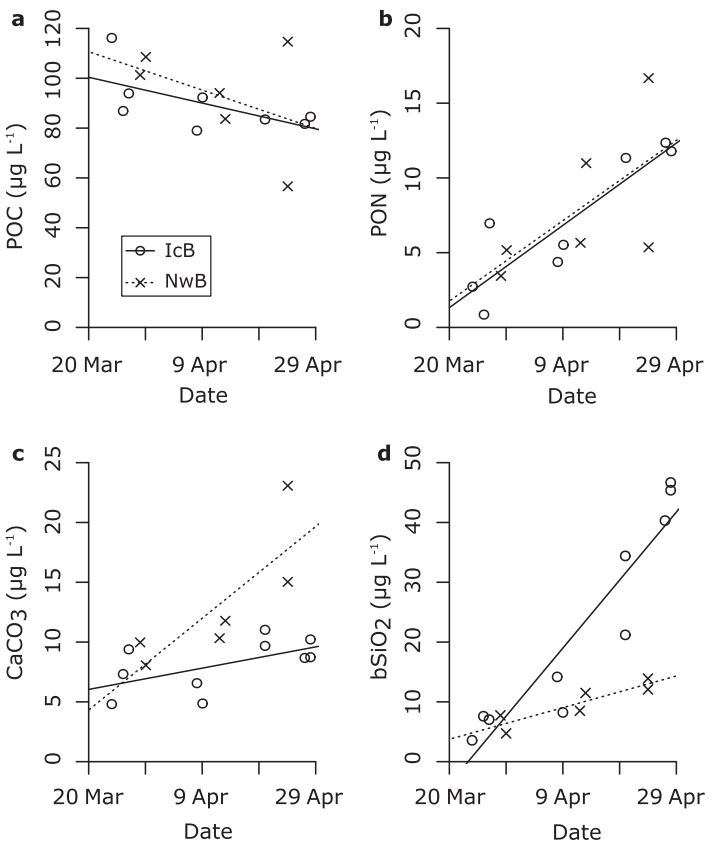

Figure 3. Total (suspended + small sinking) particle concentrations of (a) POC, (b) PON, (c) $CaCO_3$, and (d) $bSiO_2$ in the upper 200 m in the IcB (circles) and NwB (crosses). The trend of concentration change over time is shown by lines (solid and dotted, respectively).

The amount of carbon transported by a given particle ("mass flow rate"; μg d^{-1}) was calculated using its carbon content ($m_{particle}$; μg POC) and the time needed for the particle to sink the height of the MSC (h; 1.5 m) according to its measured sinking speed ($v_{particle}$; m d^{-1}) (see section 2.2). Particles whose sinking speed was not measured directly were assumed to sink with the median sinking speed of particles at the particular station and visit (82–97 m d^{-1}). Mass flow rates of all particles collected during a MSC deployment were then summed and normalized to area using the area of the MSC base (A_{MSC}; 0.06 m^2).

To account for the uncertainties and potential error propagation, all concentrations and fluxes were estimated using the Monte Carlo method (see supporting information).

2.5. Video Plankton Recorder

High-resolution images of particles were obtained using a

digital autonomous Video Plankton Recorder (VPR). The VPR (DAVPR-15, Seascan Inc., USA) is a modern underwater camera system towed by the research vessel. The VPR was equipped with a high-resolution camera (1 mega pixel (1024 × 1024) Uniq UC-1830CL color camera) which records approximately 15 image frames s^{-1}. We used a camera setting with a field of view of 24 × 24 mm resulting in a calibrated image volume of 44.72 mL. Illumination for the camera was provided by a strobe light which was synchronized with the camera shutter. Additionally, the VPR was equipped with a CTD (Seabird SBE-49, Seabird, USA) to obtain hydrographic information. The VPR was mounted on an equipment rack with a v-fin depressor and deployed vertically from near surface to its maximum depth rating (1200 m). Recorded images and sensor data were saved to the instruments hard drive and retrieved after each deployment. Plankton and particle images were extracted from each image frame as region of interest (ROIs) using the Autodeck image analysis software (Seascan Inc., USA) and saved as TIFF files. Each ROI was tagged using a timestamp to allow merging with the hydrographic and depth information that were written to a separate logfile.

All images were classified automatically following a method by *Hu and Davis* [2006] as described in *Möller et al*. [2012]. Images of particles were combined in one marine snow category varying in shape and size and yielded high classification accuracy due to their distinct shape and texture. However, all particles were additionally manually double-checked after classification. Finally, size (as ESD) was extracted from each 2-D image and particle abundances were calculated and averaged for VPR deployments in temporal proximity using the same depth bins that were used for the MSC. Smallest particles had ESDs of 0.1 mm, allowing direct comparison of VPR and MSC data.

2.6. Net Surface Heat Flux

The Net Surface Heat Flux (NSHF) is a commonly used indicator for assessing convective mixing [e.g., *Taylor and Ferrari*, 2011]. Heat loss at the sea surface (defined here as negative NSHF) increases the density of

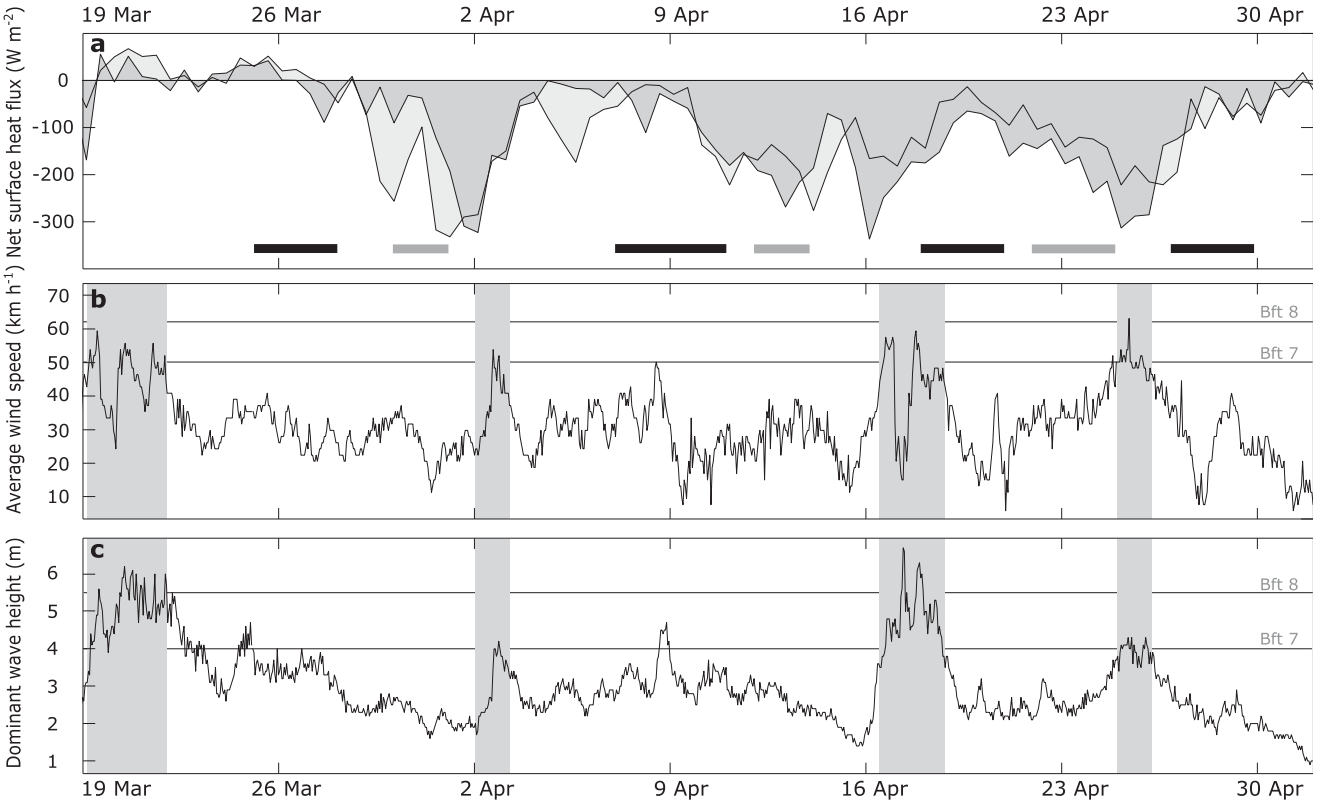

Figure 4. (a) Net surface heat flux in the IcB (dark gray area) and NwB (light gray area). Black and gray bars near *x* axis identify periods during which the respective station was sampled. (b) Average wind speed and (c) dominant wave height at the K5 buoy (59.04°N, 11.25°W). Gray areas show periods of severe weather. Lines show lower thresholds for force 7 and 8 on the Beaufort scale.

surface waters and thus induces water column instability and convective mixing. The NSHF was calculated according to

$$\mathrm{NSHF} = \mathrm{SW_{in}} - \mathrm{LW_{out}} - \mathrm{HF_{sens}} - \mathrm{HF_{lat}}, \quad (5)$$

where SW_{in} is the incoming short-wave radiation, LW_{out} the outgoing long-wave radiation, HF_{sens} the sensitive heat flux, and HF_{lat} the latent heat flux, which were obtained from the ECMWF ERA Interim reanalysis data set [*Dee et al.*, 2011].

3. Results

3.1. Phytoplankton Community

At both sites the bloom began ~20 days after the study ended according to satellite-derived maps of Chl concentration and "traditional" bloom metrics (5% increase in surface Chl above annual median) [*Daniels et al.*, 2015]. This suggests that both plankton communities represented early stages of the North Atlantic bloom. However, the plankton community structures at the two sites were different, with diatoms dominating the IcB and nano and picoplankton dominating the NwB [*Daniels et al.*, 2015]. The difference in the developing community structure was also reflected in the strong increase of PON at both sites, the pronounced increase in $bSiO_2$ concentrations in the IcB and moderate increases of both $bSiO_2$ and $CaCO_3$ concentrations in the NwB (Figure 3).

Details of the microbial community and microzooplankton grazing during our cruise are discussed, respectively, by *Paulsen et al.* [2015] and *Morison and Menden-Deuer* [2015].

3.2. Hydrographic Setting and Chlorophyll-a Distribution

Warming of the upper ocean was observed for about 1 week immediately at the beginning of the cruise (20–27 March). Thereafter, daily mean NSHF was negative, indicating heat leaving the ocean at both stations for the remaining period of the cruise (Figure 4a). High winds (Beaufort scale 7) were observed on three occasions (around the 2 April, 17 April, and 25 April). Around the 17 April, winds were very strong (with gusts of 10 Beaufort) and waves exceeded 6 m in height (Figures 4b and 4c).

The IcB was characterized by a MLD of ~660 m (range 602–767 m) throughout the cruise. However, close examination of the density and temperature profiles of the upper 100 m revealed a weak, unstable stratification. The mixing layer depth was shallower during the first two visits (27–96 and 6–42 m, respectively) and

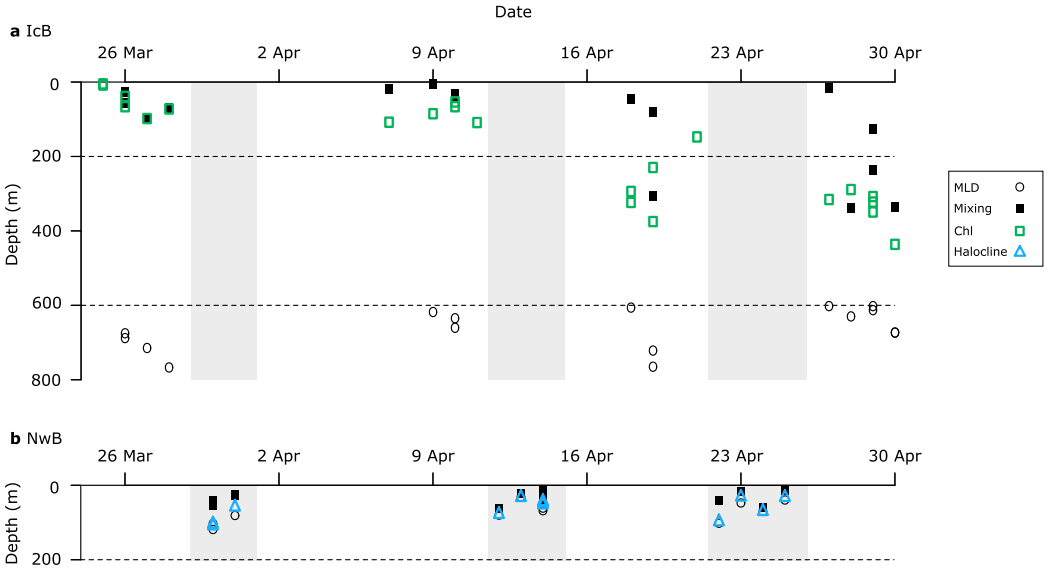

Figure 5. Changes of stratification during our study in the (a) IcB and (b) NwB, showing mixed-layer depth (MLD, circles), mixing layer depths (solid squares), the depths below which Chl was <0.25 mg m^{-3} in the IcB (green squares), and the halocline (depth at which salinity was 0.05 psu lower than at 5 m depth) in the NwB (blue triangles). Light gray areas show periods of sampling in the NwB.

deeper during the last two visits (45–307 and 15–337 m, respectively) (Figure 5). A clear Chl maximum was present in the upper 50 m during the 1 and 2 visit (Figures 6a and 6b). However, during the third visit the Chl profile in the upper 50 m had decreased by ~25% and Chl concentrations between 50 and 350 m were three times higher than during the previous visit (Figure 6c). This redistribution of Chl throughout the upper 400 m occurred during a 9 day period before the third visit during which there was a strong storm (9–10 on Beaufort wind force scale; Figure 4). Vertical profiles had changed little when we returned 8 days later for the fourth visit (Figure 6d). For the interpretation of our data, we therefore divided the sampling period in the IcB into two phases, prestorm (25 March–10 April) and poststorm (19 April–29 April).

In contrast, the water characteristics at the station in the NwB changed little during the three visits (Figures 5 and 6e–6g). The station was located in the frontal zone between North Atlantic Current and East Icelandic Current. At the Eastern corner of the Faroe Plateau, the Atlantic Water (AW) flows northeast across both the Lower Arctic Intermediate Water (LAIW) located at 250–500 m depth and the Norwegian Sea Deep Water (NSDW) located below 600 m (Figure 1c). The two salinity minima at ~200 and 600 m are likely associated with the North Icelandic Winter Water (NIWW) and the deep Arctic Intermediate Water (AIWd) [*Blindheim*, 1990]. We suspect that the strong stratification at the NwB was caused by the AW flowing over the NIWW rather than the development of a seasonal thermocline; salinity profiles showed a drop in salinity from 35.18 psu below ~50 (20–70) m depth (associated with AW) to ~34.92 psu at 200 m (associated with NIWW; compare to Figure 1c). A comparison between the depth at which salinity dropped 0.05 psu below that at 5 m depth and the MLD shows that both metrics give approximately the same depth (linear regression with slope = 0.99 and an intercept not significantly different from 0; $P < 0.01$, $R^2 = 0.89$, n = 12; see also Figure 5). This MLD was ~70 m (range: 32–119 m). The mixing layer depth was shallower with an average of 38 m (range: 15–68 m). Surface Chl increased between visits from an initial 0.58–0.59 to 0.84–0.93 μg Chl L^{-1}, driven by an increase in the 2–10 μm size fraction [*Daniels et al.*, 2015].

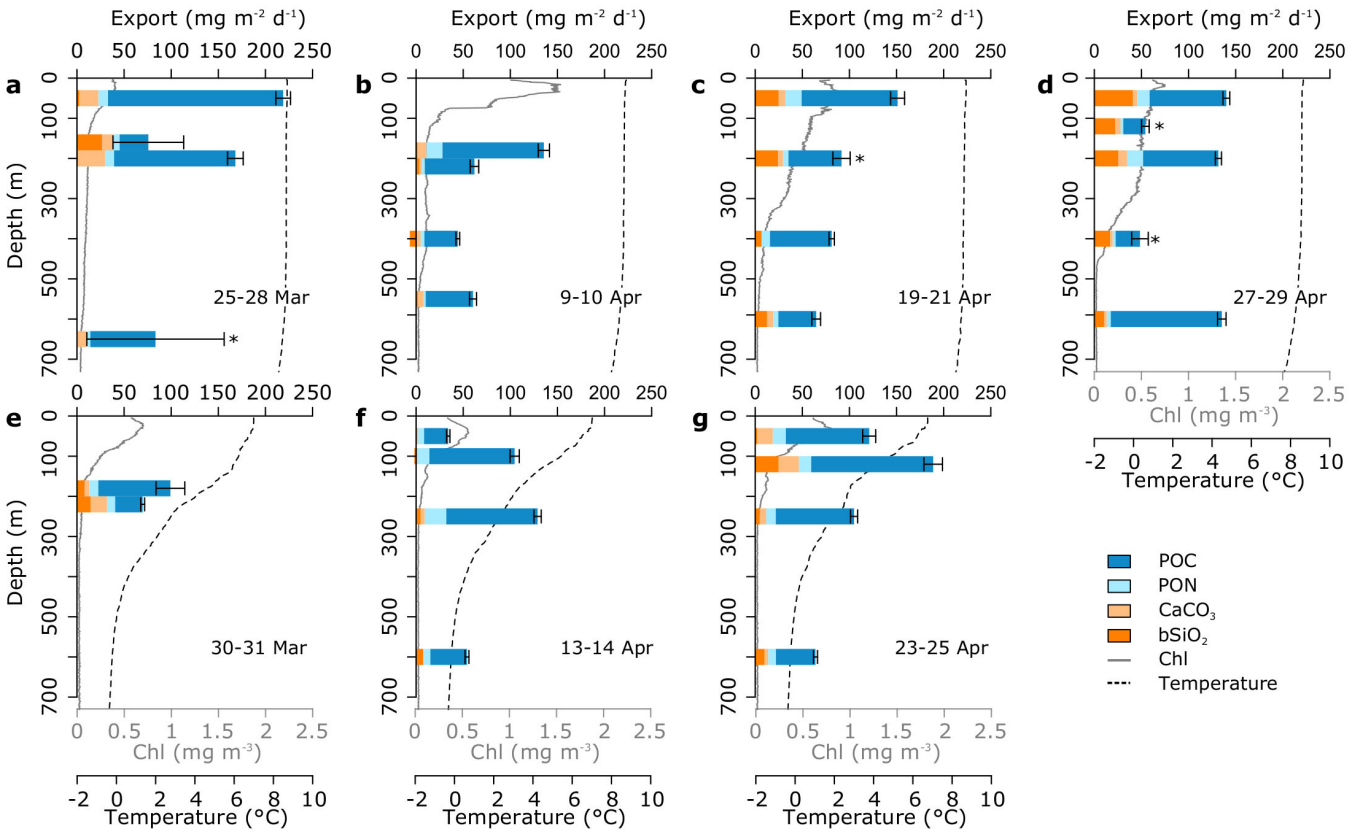

Figure 6. Flux profiles of POC (deep blue), PON (light blue), $CaCO_3$ (light orange), and $bSiO_2$ (deep orange) observed during four visits in the IcB (in order a–d) and three visits in the NwB (in order e–f). Asterisks indicate where POC fluxes were calculated from $CaCO_3$ and $bSiO_2$ flux (see section 2.4). Average Chl and temperature during each visit based on CTD profiles are shown by gray solid line and black dashed line, respectively.

3.3. Concentrations of Small Sinking and Suspended Particles

Concentrations of small sinking and suspended particles are summarized in Table 1. In the IcB, total (suspended + small sinking) POC concentration in the upper 200 m were lower at the end of the cruise (~80 μg L^{-1}) than at the start (~100 μg L^{-1}; Figure 3a). Upper ocean PON concentrations increased over time from ~2 to 12 μg L^{-1} at a rate of 0.08 day^{-1} of the initial concentration (Figure 3b). Upper ocean concentrations of total $CaCO_3$ were slightly higher at the end of the cruise, increasing from ~6 to ~10 μg L^{-1} (Figure 3c). Upper ocean $bSiO_2$ concentrations showed the most pronounced change over time, increasing from 6 to 44 μg L^{-1} with a rate of 0.19 day^{-1} (Figure 3d). In the NwB, total particle concentrations of POC and PON in the upper 200 m followed similar trends to those observed in the IcB (Figures 3a and 3b). $CaCO_3$ concentrations, in contrast, increased from 9 to 19 μg L^{-1} (0.04 day^{-1}), and $bSiO_2$ concentrations increased from 6 to 13 μg L^{-1} (0.04 day^{-1}; Figures 3c and 3d).

The relative contribution of small sinking matter to total (suspended + small sinking) matter varied for the different components. For POC, small sinking particles contributed 6 ± 3% and 5 ± 4% to total POC in the IcB and NwB, respectively. For PON, $CaCO_3$, and $bSiO_2$ the respective contribution of small sinking particles was 14 ± 15% and 13 ± 12% (PON), 6 ± 5% and 4 ± 3% ($CaCO_3$), and 5 ± 9% and 5 ± 5% ($bSiO_2$).

3.4. Fluxes of Small Particles

POC flux carried by small particles (average ± S.D.) in the IcB and NwB were of similar magnitude with 74 ± 44 and 70 ± 34 mg POC m^{-2} d^{-1}, respectively. For PON, $CaCO_3$, and $bSiO_2$, the respective fluxes at the two sites were 8 ± 5 and 11 ± 5 mg PON m^{-2} d^{-1}, 9 ± 7 and 8 ± 8 mg $CaCO_3$ m^{-2} d^{-1}, and 13 ± 13 and 8 ± 8 mg $bSiO_2$ m^{-2} d^{-1}. Upward fluxes were observed for $bSiO_2$ during two occasions (Table 1).

In the IcB, small particle fluxes varied considerably in magnitude and did not show a clear trend with depth or over time, though fluxes at ~600 m were generally lower than fluxes observed at 50 m (Figures 6a–6d and Table 1). In the NwB, small particle fluxes were highest in the upper 250 m and appeared to decrease with depth (Figures 6e–6g). Fitting of a power law function ($Fz = F_{MLD} \times (z/MLD)^{-b}$) [*Martin et al.*, 1987]) to the bootstrapped (n = 10,000) data for small-particle POC flux below the maximum recorded MLD (93 m) showed a moderate fit ($P = 0.09$, $R^2 = 0.39$, n = 8) with an average exponent b of 0.50 (±0.25 S.D.).

3.5. Large Particle Sizes, Concentrations, and Fluxes

The average size of large particles at any one depth or station ranged from 0.11 to 0.42 mm ESD with no apparent trend over time or with depth (Table 2). Estimates of average particle size by MSC and VPR were similar, although average estimates of ESD based on MSC samples tended to be smaller than those based on VPR records (see supporting information).

Concentrations of large particles as estimated by the MSC and VPR ranged from 0 to 70 particles L^{-1} (Table 2). MSC and VPR estimates differed at times by an order of magnitude. This discrepancy might be caused by the low sampling volume (95 and ~250 L, respectively; Table 2), the potential patchiness of particles, and temporal offsets between VPR and MSC deployments (see supporting information for a detailed discussion). Concentrations of large particles decreased with depth at all stations according to measurements from both the VPR and MSC, with the exception of MSC-based estimates in the IcB on 19 April. At this station the MSC collected a relatively large number of particles at 600 m (5.1 particles L^{-1}; Table 2). During the course of the cruise, particle concentrations increased at both stations toward a maximum of 70 particles L^{-1} at 50 m in the IcB on 28 April.

Large particle sinking speeds ranged from 3 to 736 m d^{-1} with a median sinking speed of 88 m d^{-1} (interquartile range: 69–104 m d^{-1}, see also Table 2). Estimated fluxes based on the MSC ranged from 0 to 48 mg POC m^{-2} d^{-1} reflecting the temporal and vertical changes observed for particle concentrations: an increase over time at both stations and a decrease of fluxes with depth in the NwB (Table 1). Based on the MSC, large particles contributed ≤15% of the total POC flux except for on three occasions: on 19 April when a large number of particles was collected at 600 m (contributing 54% of the total POC flux), and at 50 m in the NwB on both 14 April and 25 April (contributing 28% and 17% of the total POC flux, respectively). Large particles collected by the MSC were not photographed during the last visit at the IcB (27–19 April). According to the VPR, large particles were very abundant during this visit, thus potentially making up the bulk of the flux.

Table 2. Average Particle Size and Concentration of Large Particles in the Iceland Basin (IcB) and Norwegian Basin (NwB) as Recorded by the VPR[a]

						Average Size		Concentration		Average Size			Sinking Speed	
Station	Visit	Date	Depth (m)	Sampling Volume (L)	VPR Time in Bin (min)	(ESD mm)	(S.D.)	(Particle L^{-1})	(S.D.)	(ESD mm)	(S.D.)	Concentration (Particle L^{-1})	(m d^{-1})	(S.D.)
IcB	1	28 Mar 12	25–75	211	5.24	0.25	0.07	0.47	0.09			0		
IcB	1	28 Mar 12	150–200	115.4	2.9	0.39	0.18	0.03	0.02			0		
IcB	1	28 Mar 12	175–225	124.4	3.09	0.22	0.20	0.01	0.01			0		
IcB	1	28 Mar 12	625–675	342.6	8.51	0.29	0.04	0.01	0.01			0		
IcB	2	10 Apr 12	175–225	250.9	6.3	0.19	0.06	0.87	0.14	0.21	0.12	0.07	59	19
IcB	2	10 Apr 12	375–425	255.1	6.4	0.24	0.10	0.11	0.04	0.15	0.03	0.06	69	33
IcB	2	10 Apr 12	525–575	260.5	6.5	0.27	0.15	0.03	0.02	0.26	0.15	0.11	90	19
IcB	3	21 Apr 12	25–75	277.3	6.8	0.28	0.02	24.38	4.66	0.23	0.18	1.83	134	167
IcB	3	21 Apr 12	175–225	248.3	6.2	0.42	0.28	4.25	2.2	0.33	0.18	0.08	105	61
IcB	3	21 Apr 12	375–425	249.9	6.2	0.24	0.11	0.92	0.45	0.34	0.25	0.08	113	111
IcB	3	21 Apr 12	575–625	249.8	6.2	0.30	0.18	0.18	0.11	0.16	0.05	5.10	140	124
IcB	4	28 Apr 12	25–75	244.8	6.1	0.22	0.05	69.46	7.65					
IcB	4	28 Apr 12	95–145	245.6	6.1	0.31	0.04	12.08	3.31					
IcB	4	28 Apr 12	175–225	252	6.3	0.30	0.12	7.95	6.5					
IcB	4	28 Apr 12	375–425	249.2	6.2	0.12	0.10	15.61	6.11					
IcB	4	28 Apr 12	575–625	257.5	6.4	0.30	0.14	0.42	0.29					
NwB	1	31 Mar 12	175–225	145.1	3.6	0.33	0.03	0.29	0.05			0		
NwB	2	14 Apr 12	25–75	265.4	6.6	0.31	0.05	0.53	0.09	0.15	0.03	1.07	113	44
NwB	2	14 Apr 12	75–125	290.3	7.2	0.19	0.04	0.09	0.08	0.18	0.05	0.17	101	72
NwB	2	14 Apr 12	225–275	268.2	6.9	0.40	0.23	0.12	0.03	0.27	0.08	0.09	113	65
NwB	2	14 Apr 12	575–625	285	7.7	0.29	0.11	0.01	0.05			0		
NwB	3	24 Apr 12	25–75	279.8	6.9	0.33	0.06	0.82	0.36	0.12	0.03	2.75	75	0
NwB	3	24 Apr 12	95–145	252	6.2	0.21	0.15	0.18	0.15	0.21	0.12	0.11	85	52
NwB	3	24 Apr 12	225–275	218.8	5.4	0.29	0.11	0.14	0.11	0.18	0.09	0.13	79	26
NwB	3	24 Apr 12	575–625	211.1	5.2	0.37	0.22	0.01	0.03	0.14	0.06	0.02	49	37

[a]These are compared to large particles collected using the MSC at the same site, visit, and approximate depth.

4. Discussion

4.1. Prebloom Particle Composition and Flux Rates of Small Sinking Particles

The POC flux rates of small particles in the upper 200 m ranged from 23 to 186 mg POC m^{-2} d^{-1}, similar to total particle fluxes observed using sediment traps during (10–152 mg POC m^{-2} d^{-1} at 150–750 m depth [*Buesseler et al.*, 1992; *Martin et al.*, 2011]) and after the North Atlantic spring bloom (29–182 mg POC m^{-2} d^{-1} [*Riley et al.*, 2012; *Giering et al.*, 2014]). A comparison with previous studies that measured particle flux using sediment traps or MSCs in the North Atlantic (45°N–75°N [*Buesseler et al.*, 1992; *Martin et al.*, 2011; *Riley et al.*, 2012; *Torres-Valdes et al.*, 2014, and references therein]) shows that our prebloom flux rates fall well within the expected range both with season (Figure 7a) and with depth (Figure 7b). Moreover, our fluxes were similar to estimates based on optical backscattering profiles measured by Bio-Argo floats in the Norwegian Sea [*Dall'Olmo and Mork*, 2014]. *Dall'Olmo and Mork* [2014] investigated seasonal patterns in POC export fluxes by small (approximately 0.2–20 μm) particles and calculated that highest fluxes occurred at the time of mixed-layer shoaling, with fluxes as high as 250 mg POC m^{-2} d^{-1} at ~100 m depth.

In order to establish whether our estimated fluxes are plausible, we compared export fluxes to both production rates and the standing stock of POC present at the time of sampling. Absolute concentrations of POC in the upper 200 m decreased over the duration of the cruise at both stations whereas the concentrations of PON, $CaCO_3$, and $bSiO_2$ all progressively increased (Figure 3). These data suggest that although absolute concentrations of particulate organic matter in the upper ocean decreased, the relative abundance of living phytoplankton increased over the period of sampling [see also *Daniels et al.*, 2015]. Primary production rates, measured using the ^{13}C technique and integrated over the euphotic zone (50–115 m deep), ranged between 38 and 359 mg C m^{-2} d^{-1} [*Daniels et al.*, 2015] and were thus of the same order of magnitude as our flux estimates in the upper 200 m (23–186 mg POC m^{-2} d^{-1}). Based on interpolation of the integrated standing stocks of small sinking particle POC between 50 and 600 m, we estimated standing stocks of 1.9 and 2.1 g m^{-2} in the IcB and NwB, respectively. The observed fluxes at 600 m (on average 73 and 40 mg POC m^{-2} d^{-1}, respectively) were equivalent to 2–4% of this standing stock. It follows that flux rates even higher than those that we observed could have been readily sustained by the ecosystems at the two sites.

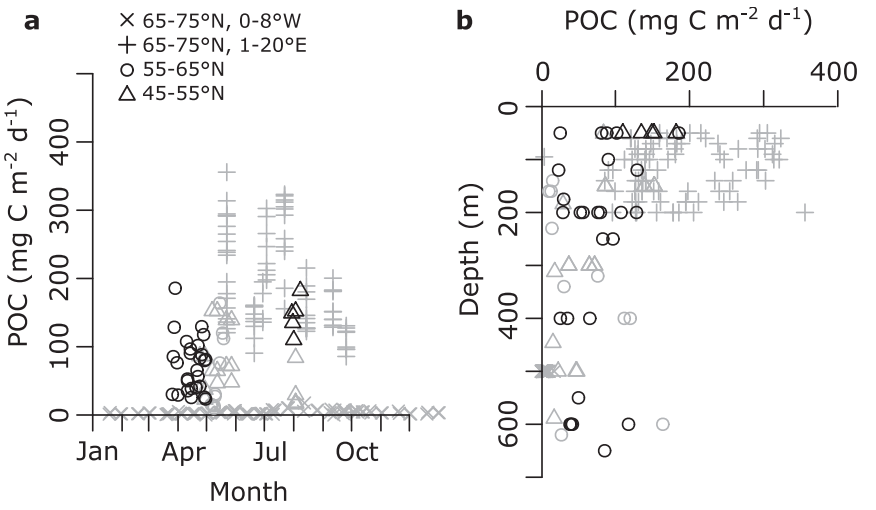

Figure 7. POC fluxes in the North Atlantic (45°N–75°N) measured using MSCs (black symbols) and sediment traps (gray symbols) [*Buesseler et al.*, 1992; *Martin et al.*, 2011; *Riley et al.*, 2012; *Torres-Valdes et al.*, 2014, and references therein]. Fluxes are plotted against (a) month and (b) depth. Symbols indicate geographical region as in legend. Data presented in this paper are shown by black circles.

These high fluxes need to be reconciled with previous studies based on deep traps that observed low fluxes during and prior to the spring bloom period [*Honjo and Manganini*, 1993]. Long-term sediment trap data from 3000 m at the Porcupine Abyssal Plain (49°N, 16°W), for example, suggest that prebloom deep flux rates are small (2–4 mg POC m^{-2} d^{-1}) and deep fluxes only increase after surface Chl concentrations have peaked (based on 14 years of data at 3000 m depth [*Lampitt et al.*, 2010]). This is likely because bloom or postbloom export events are often dominated by fecal pellets [*Turner*, 2002, and references therein] and larger phytodetritus aggregates [e.g., *Lampitt et al.*, 2001], which form during periods of high phytoplankton concentration [e.g., *Kiørboe et al.*, 1994; *Jackson and Kiørboe*, 2008] or toward the end of a bloom when nutrients are limiting [e.g., *Smetacek*, 1985; *Armbrecht et al.*, 2014]. These large aggregates sink rapidly (>100 m d^{-1}) through the mesopelagic [e.g., *Lampitt et al.*, 2001; *Martin et al.*, 2011] and can, at times, reach the abyssal plain in large quantities [e.g., *Lampitt et al.*, 2001]. Our observed prebloom fluxes, on the other hand, consisted mainly of small sinking particles, which likely sank at average speeds of ~20 m d^{-1}. These small particles are potentially rich in labile organic compounds [*Lee et al.*, 2000; *Sheridan et al.*, 2002; *Alonso-Gonzalez et al.*, 2010] and are therefore readily colonized and remineralized by mesopelagic organisms [*Mayor et al.*, 2014]. The slow sinking rates of small particles imply that the majority will be remineralized within the mesopelagic [*Villa-Alfageme et al.*, 2016] and thus that the export fluxes we observed are unlikely to reach lower bathyal or abyssal depths.

We next discuss the potential mechanisms driving export of small-sinking particles at our two study sites, which exhibited markedly different hydrographic conditions.

4.2. Particle Transport Mechanisms From a Deep Mixed Layer (IcB)

Positive NSHF into the oceans reduces mixing and ultimately leads to the development of stratification. However, following a period of positive NSHF, the physical profile of a previously deeply mixed environment does not change immediately and can falsely indicate deep convection for days or potentially weeks [*Marshall and Schott*, 1999; *Taylor and Ferarri*, 2011]. During such a period, a shallower, actively "mixing layer" may develop [*Brainerd and Gregg*, 1995], allowing surface phytoplankton concentrations to increase despite a deep "mixed layer" and the lack of obvious physical stratification [e.g., *Townsend et al.*, 1992]. We observed Chl concentrations in the IcB peaked at the surface even though the water column appeared to be mixed to ~700 m (Figure 4). Together with the NSHF, which remained generally positive during the week before our study, and a shallow mixing layer (~44 m), this indicates that deep mixing at the IcB had abated sufficiently for the phytoplankton population to establish near the surface.

Yet this stratification was weak and unstable. Half-way through our 7 week long study, we observed severe weather conditions (Beauford Scale 9-10). After this storm, surface Chl concentrations in the IcB had

decreased to $<$1.2 mg Chl m^{-3} and remained low for the rest of the cruise at concentrations similar to those found in the NwB (0.62–1.18 versus 0.84–0.93 mg Chl m^{-3}, respectively [*Daniels et al*., 2015]). Much of the Chl appeared to have been distributed over the upper 300–400 m (Figures 5, and 6c,d). It has previously been suggested that storms are a potential driver for prebloom export. *Koeve et al*. [2002] found, in 1992, that the developing spring bloom in the Northeast Atlantic was interrupted by storm events which lead to the export of around half of the standing stock. After the storm at the IcB, we observed high POC fluxes driven by small sinking particles as deep as 600 m and a redistribution of Chl down to ~400 m Figures 5, and 6c,d. We can think of two possible mechanisms that could cause such a scenario: 1) sinking of large particles that had aggregated during the storm and subsequent disaggregation at depth, or (2) deep mixing of small particles during the storm ("the mixed-layer pump").

Aggregation and Disaggregation. Aggregation is controlled by several parameters, including cell concentration, cell size, shear, and mixing layer depth [*Jackson and Lochmann*, 1992]. Using a numerical model, *Jackson and Lochmann* [1992] showed that aggregation can occur at relatively low phytoplankton concentrations when shear is high. *Kiorboe et al*. [1994] tested this model using field data from a shallow Danish fjord and calculated that during periods of high shear ($\geq$1.2 s^{-1}) the critical concentration for aggregation of diatom species with a diameter of ~20 μm was between 50 and 400 cells mL^{-1}. During our study, diatom abundance in the IcB increased rapidly between the first and the second visit from 1.3 to 250 cells mL^{-1}, of which ~50% were $\geq$20 μm in diameter [*Daniels et al*., 2015]. It is thus feasible that large aggregates formed during the storm and subsequently sank to depth. Indeed, after the storm, large particle concentrations in the upper 100 m were 2 orders of magnitude higher than before the storm (Table 2).

Large particle concentrations were highest during the fourth visit at the IcB, even though Chl concentrations and primary production rates had decreased since the third visit [*Daniels et al*., 2015]. *Jackson and Lochmann* [1992] suggested that a deeper mixing layer enables the formation of larger aggregates compared to shallower mixing layers. This is because a deeper mixing layer allows large aggregates to interact with smaller ones for longer, resulting in even larger, faster sinking aggregates. Although we observed a deep mixing layer and highest particle concentrations during the fourth visit, we did not observe an increase in large particle size, and large particles remained relatively small with ~0.3 mm ESD (Table 2).

Aggregates formed in the surface ocean can disaggregate at depth via mechanical fragmentation, dissolution, or zooplankton activity, thus generating small particles at depth [*Stemmann et al*., 2004]. After the storm in the IcB, concentrations of large particles decreased rapidly with depth (Table 2), which could indicate that particle disaggregation took place. However, concentrations of suspended and/or small sinking particles did not increase with depth (Table 1), suggesting that the dominant reason for the disappearance of large particles was remineralization (e.g., by particle-attached microbes [*Iversen and Ploug*, 2010; *McDonnell et al*., 2015; A. Belcher et al., submitted manuscript, 2016]) or that disaggregation occurred at a similar rate as remineralization of suspended and small sinking particles.

While aggregation/disaggregation can explain the high POC fluxes by small sinking particles at depth and the redistribution of Chl to ~400 m, a similar pattern could be caused by deep mixing.

Mixed-Layer Pump. The "mixed-layer pump" [*Gardner et al*., 1995] could be important prior to the spring bloom, the start of which begins when the increase in phytoplankton biomass appears to accelerate. Prior to the establishment of a spring bloom, a period exists in which the upper ocean is in transition; short periods in which the ocean stratifies and phytoplankton production increases are interrupted by returns to the deep mixing via convection or increased surface wind stress [*Ho and Marra*, 1994]. During this mixed-layer deepening, "new" phytoplankton cells containing "newly fixed" carbon can be transported to deeper regions with lower concentrations of organic carbon. When the water column next restratifies, some of these cells are trapped below the mixed layer and, owing to the cessation of mixing, start to slowly sink to depth ("detrainment"). This export mechanism does not rely on particle aggregation and may be an important export term [*Ho and Marra*, 1994; *Körtzinger et al*., 2008]. Moreover, for the mixed-layer pump the sinking speed of particles is no longer a necessary determinant over the penetration depth, as the bursts of deep mixing transport particles down several hundreds of meters at a much faster rate than would occur via sinking alone. The two components of the transition period, stratification and mixing, support export of organic matter as the stratified period promotes phytoplankton growth and the mixing period provides rapid export.

We observed precisely such an event series in the IcB. We suggest that the storm in conjunction with the negative NSHF (Figure 4) induced strong mixing in the IcB and subsequent mixing-layer deepening (Figure 5). If physical deep mixing was responsible for the redistribution of Chl, both should be closely linked. Indeed, during the fourth visit Chl concentrations were nearly constant over the upper 300 m (Figure 6d). Moreover, when comparing the depth distribution of Chl (the depth at which Chl concentrations were $>$0.25 mg m^{-3}) and the depth of the mixing layer, there appears to be a strong correlation (Figure 5). Thus, high fluxes of small sinking particles at depth could have been facilitated by deep mixing.

Regardless of the mechanism, if our cruise was followed by a period of positive NSHF, the mixing layer would have shoaled again, and the particles at depth could have been detrained. We try to estimate the amount of carbon this mechanism would supply to the mesopelagic. During the third and fourth visit, small sinking particles, integrated over 50–600 m depth (Table 1), contained 2.0–2.7 g POC m^{-2}. Alternatively, we can use Chl as an indicator for fresh biomass that had been redistributed to depth after the storm. Based on Chl profiles and assuming a C:Chl ratio of 40 mg:mg [*Poulton et al*., 2010], integrated Chl-C (50–600 m depth) could supply 6.4 g C m^{-2} to the mesopelagic. Considering that daily export fluxes rarely exceed 300 mg C m^{-2} d^{-1} (Figure 7), these integrated stocks are very large and equivalent to 7–21 days of peak export rates. Prebloom export could thus provide significant amounts of organic carbon to the mesopelagic biota, alert the ecosystem to the forthcoming bloom, and help to close mesopelagic carbon budgets [*Giering et al*., 2014].

4.3. Particle Export From a Shallow Mixed Layer (NwB)

Gardner et al. [1995] suggested that the mixed-layer pump could be important in regions with shallow mixing layers ($\sim$50 m depth) and relatively modest changes in mixing layer depth (10 m). Yet this mechanism is likely important only if the mixing layer deepens much slower than particles sink (e.g., in our case at rates higher than 20 m d^{-1}). Otherwise, particles that had been detrained during mixing-layer shoaling would be entrained during mixing-layer deepening, and would not necessarily lead to an increased export of organic matter. In the NwB, the storm had no obvious effect on the water column or particle fluxes, likely because of the strong stratification. Yet we observed changes of the mixing layer at rates of $\sim$44 m d^{-1} (range: 3–84 m d^{-1}) throughout the study. Owing to the strong oscillations in mixing-layer depth, it is likely that mixing would have negated any previous downward transport and detrainment of particles.

The concentrations of all particle fractions (suspended, small sinking, and large sinking) decreased with depth (Tables 1 and 2). We therefore suggest that particle export at the NwB followed the "traditional" mechanisms and the observed fluxes by small sinking particles likely resulted from disaggregation: particles aggregated in the mixed layer until they reached a critical density that allowed them to sink out of the mixed layer [*Jackson and Lochmann*, 1992; *Burd and Jackson*, 2009], followed by disaggregation and remineralization at depth [e.g., *Burd and Jackson*, 2009; *Giering et al*., 2014]. It is noteworthy, however, that Chl concentrations in the mixing layer were much lower than in the IcB (0.6–0.9 mg Chl m^{-3}) and the phytoplankton community was dominated by nano and picoplankton [*Daniels et al*., 2015], reducing the likelihood for aggregation [*Jackson and Lochmann*, 1992]. Overall, the penetration depth of small sinking particles in the NwB was shallower than in the IcB by several hundreds of meters.

5. Conclusion

We present the first depth profiles of small ($<$0.1 mm ESD) sinking particles before the North Atlantic spring bloom. The rate of export via small sinking particles was very high with POC fluxes being comparable to rates observed during and after the spring bloom. The observed prebloom particle dynamics differed from those during the North Atlantic spring bloom [e.g., *Lampitt et al*., 2001; *Martin et al*., 2011] as a significant fraction was in form of small sinking particles, which likely sank at average speeds of $\sim$20 m d^{-1}. This result contradicts the traditional view that prespring bloom export is negligible.

Our data suggest two export mechanisms for slow sinking particles in two contrasting environments. In the NwB, small sinking particles likely reached the upper mesopelagic by disaggregation of larger, faster sinking particles. In the IcB, our observations support the hypothesis of early-spring export via small, slow-sinking particles due to intermittent destabilization of the water column [*Ho and Marra*, 1994; *Körtzinger et al*., 2008]. In early spring, changes in NSHF favor the temporary development of a surface Chl maximum. During

a period of high winds and negative NSHF, this stratification is broken down and the "fresh" phytoplankton cells are mixed to depth. Subsequent restratification could trap these small particles at depth ("detrainment") and lead to high particle fluxes at depth without the need for aggregation ("mixed-layer pump" [*Gardner et al*., 1995]).

Yet the observed prebloom fluxes were unlikely to penetrate into the bathypelagic zone as they were largely based on slow-sinking cells and aggregates, which were likely rich in labile organic compounds and therefore readily consumed by the resident biota. Prebloom export may be an important source of carbon for the mesopelagic biota, potentially alerting the ecosystem to the forthcoming spring bloom.

Acknowledgments
Captain, crew, and scientist of the FS *Meteor* during cruise M87/1. F. Morison for the microscope camera. Satellite images were kindly provided by B. Taylor at the NERC Earth Observation Data Acquisition and Analysis Service (NEODAAS). We thank Sharon McNeill (Scottish Association for Marine Science) for her support with C and N measurements. Data on wind speed and wave height are provided by the Met Office (http://www.metoffice.gov.uk) and were licensed under the Open Government Licence. The "Deep Convection" cruise was funded by the Deutsche Forschungsgemeinschaft. Financial support for the observations reported in this paper was provided by the FP7 program EURO-BASIN (contract 264933). The work was further supported by NERC National Capability funding. The data for this paper are available at http://doi.pangaea.de/10.1594/PANGAEA.826220.

References

Acuña, J., M. López-Alvarez, E. Nogueira, and F. González-Taboada (2010), Diatom flotation at the onset of the spring phytoplankton bloom: An in situ experiment, *Mar. Ecol. Prog. Ser.*, *400*, 115–125, doi:10.3354/meps08405.

Alldredge, A. (1998), The carbon, nitrogen and mass content of marine snow as a function of aggregate size, *Deep Sea Res., Part I*, *45*(4–5), 529–541, doi:10.1016/S0967-0637(97)00048-4.

Alldredge, A. L., and M. W. Silver (1988), Characteristics, dynamics and significance of marine snow, *Prog. Oceanogr.*, *20*(1), 41–82, doi:10.1016/0079-6611(88)90053-5.

Alonso-González, I. J., J. Arístegui, C. Lee, A. Sanchez-Vidal, A. Calafat, J. Fabrés, P. Sangrá, P. Masqué, A. Hernández-Guerra, and V. Benítez-Barrios (2010), Role of slowly settling particles in the ocean carbon cycle, *Geophys. Res. Lett.*, *37*, L13608, doi:10.1029/2010GL043827.

Anderson, L., and B. Sweeney (1977), Diel changes in sedimentation characteristics of *Ditylum brightwelli*: Changes in cellular lipid and effects of respiratory inhibitors and ion-transport modifiers, *Limnol. Oceanogr.*, *22*(3), 539–552, doi:10.4319/lo.1977.22.3.0539.

Armbrecht, L. H., V. Smetacek, P. Assmy, and C. Klaas (2014), Cell death and aggregate formation in the giant diatom *Coscinodiscus wailesii* (Gran & Angst, 1931), *J. Exp. Mar. Biol. Ecol.*, *452*, 31–39, doi:10.1016/j.jembe.2013.12.004.

Belcher, A., M. Iversen, C. Manno, S. A. Henson, G. A. Tarling, and R. Sanders (2016), The role of particle associated microbes in remineralisation of faecal pellets in the upper mesopelagic of the Scotia Sea, Antarctica, *Limnol. Oceanogr.*, *61*, 1049–1064, doi:10.1002/lno.10269.

Bienfang, P. K. (1981), Sinking rates of heterogeneous, temperate phytoplankton populations, *J. Plankton Res.*, *3*(2), 235–253, doi:10.1093/plankt/3.2.235.

Blindheim, J. (1990), Arctic intermediate water in the Norwegian sea, *Deep Sea Res., Part A.*, *37*(9), 1475–1489, doi:10.1016/0198-0149(90)90138-L.

Boyd, C. M., Gradmann, (2002), Impact of osmolytes on buoyancy of marine phytoplankton, *Mar. Biol.*, *141*, 605–618, doi:10.1007/s00227-002-0872-z.

Brainerd, K. E., and M. C. Gregg (1995), Surface mixed and mixing layer depths, *Deep Sea Res., Part I*, *42*(9), 1521–1543, doi:10.1016/0967-0637(95)00068-H.

Brown, L., R. Sanders, G. Savidge, and C. H. Lucas (2003), The uptake of silica during the spring bloom in the Northeast Atlantic Ocean, *Limnol. Oceanogr.*, *48*(5), 1831–1845.

Buesseler, K. O., M. P. Bacon, J. Kirk Cochran, and H. D. Livingston (1992), Carbon and nitrogen export during the JGOFS North Atlantic Bloom experiment estimated from 234Th: 238U disequilibria, *Deep Sea Res., Part A*, *39*(7–8), 1115–1137, doi:10.1016/0198-0149(92)90060-7.

Burd, A. B., and G. A. Jackson (2009), Particle aggregation, *Annu. Rev. Mar. Sci.*, *1*, 65–90, doi:10.1146/annurev.marine.010908.163904.

Cavan, E. L., F. A. C. Le Moigne, A. J. Poulton, G. A. Tarling, P. Ward, C. J. Daniels, G. M. Fragoso, and R. J. Sanders (2015), Attenuation of particulate organic carbon flux in the Scotia Sea, Southern Ocean, is controlled by zooplankton fecal pellets, *Geophys. Res. Lett.*, *42*, 821–830, doi:10.1002/2014GL062744.

Dall'Olmo, G., and K. A. Mork (2014), Carbon export by small particles in the Norwegian Sea, *Geophys. Res. Lett.*, *41*, 2921–2927, doi:10.1002/2014GL059244.

Daniels, C. J., A. J. Poulton, M. Esposito, M. L. Paulsen, R. Bellerby, M. St. John, and A. P. Martin (2015), Phytoplankton dynamics in contrasting early stage North Atlantic spring blooms: Composition, succession, and potential drivers, *Biogeosciences*, *12*, 2395–2409, doi:10.5194/bg-12-2395-2015.

Dee, D. P., et al. (2011), The ERA-Interim reanalysis: Configuration and performance of the data assimilation system, *Q. J. R. Meteorol. Soc.*, *137*, 553–597, doi:10.1002/qj.828.

Falkowski, P. G., R. T. Barber, and V. Smetacek (1998), Biogeochemical controls and feedbacks on ocean primary production, *Science*, *281*(5374), 200–206, doi:10.1126/science.281.5374.200.

Fernández-Méndez, M., F. Wenzhöfer, I. Peeken, H. L. Sørensen, R. N. Glud, and A. Boetius (2014), Composition, buoyancy regulation and fate of ice algal aggregates in the central arctic ocean, *PLoS One*, *9*(9), e107452, doi:10.1371/journal.pone.0107452.

Flynn, K. J., and K. Davidson (1993), Predator-prey interactions between *Isochrysis galbana* and *Oxyrrhis marina*. I. Changes in particulate $\delta^{13}C$, *J. Plankton Res.*, *15*(4), 455–463, doi:10.1093/plankt/15.4.455.

Frangoulis, C., S. Belkhiria, A. Goffart, and J.-H. Hecq (2001), Dynamics of copepod faecal pellets in relation to a Phaeocystis dominated phytoplankton bloom: characteristics, production and flux, *J. Plankton Res.*, *23*(1), 75–88, doi:10.1093/plankt/23.1.75.

Gantt, E., K. Ohki, and Y. Fujita (1984), *Trichodesmium thiebautii*: Structure of a nitrogen-fixing marine blue-green alga (Cyanophyta), *Protoplasma*, *119*(3), 188–196, doi:10.1007/BF01288873.

Gardner, W. D., S. P. Chung, M. J. Richardson, and I. D. Walsh (1995), The oceanic mixed-layer pump, *Deep Sea Res., Part II*, *42*(2), 757–775, doi:10.1016/0967-0645(95)00037-Q.

Giering, S. L. C., et al. (2014), Reconciliation of the carbon budget in the ocean's twilight zone, *Nature*, *507*(7493), 480–483, doi:10.1038/nature13123.

Guidi, L., G. A. Jackson, L. Stemmann, J. C. Miquel, M. Picheral, and G. Gorsky (2008), Relationship between particle size distribution and flux in the mesopelagic zone, *Deep Sea Res., Part I*, *55*(10), 1364–1374, doi:10.1016/j.dsr.2008.05.014.

Ho, C., and J. Marra (1994), Early-spring export of phytoplankton production in the northeast Atlantic Ocean, *Mar. Ecol. Prog. Ser.*, *114*, 197–202.

Honjo, S., and S. J. Manganini (1993), Annual biogenic particle fluxes to the interior of the North Atlantic Ocean; studied at 34°N 21°W and 48°N 21°W, *Deep Sea Res., Part II*, *40*(1–2), 587–607, doi:10.1016/0967-0645(93)90034-K.

Hu, Q., and C. Davis (2006), Accurate automatic quantification of taxa-specific plankton abundance using dual classification with correction, *Mar. Ecol. Prog. Ser.*, *306*, 51–61, doi:10.3354/meps306051.
Huwaldt, J. A. (2014), Plot Digitizer, Sourceforge, U.S.A. [Available at http://plotdigitizer.sourceforge.net/.]
Iversen, M. H., and H. Ploug (2010), Ballast minerals and the sinking carbon flux in the ocean: Carbon-specific respiration rates and sinking velocity of marine snow aggregates, *Biogeosciences*, *7*(9), 2613–2624, doi:10.5194/bg-7-2613-2010.
Jackson, G. A. (1990), A model of the formation of marine algal flocs by physical coagulation processes, *Deep Sea Res., Part A*, *37*(8), 1197–1211, doi:10.1016/0198-0149(90)90038-W.
Jackson, G. A. (2005), Coagulation theory and models of oceanic plankton aggregation, in *Flocculation in Natural and Engineered Environmental Systems*, edited by I. G. Droppo, et al., pp. 271–292, CRC Press, Boca Raton, Fla., doi:10.1201/9780203485330.ch13.
Jackson, G. A., and T. Kiørboe (2008), Maximum phytoplankton concentrations in the sea, *Limnol. Oceanogr.*, *53*(1), 395–399, doi:10.4319/lo.2008.53.1.0395.
Jackson, G. A., and S. E. Lochmann (1992), Effect of coagulation on nutrient and light limitation of an algal bloom, *Limnol. Oceanogr.*, *37*(1), 77–89, doi:10.4319/lo.1992.37.1.0077.
Kiørboe, T. (2001), Formation and fate of marine snow: Small-scale processes with large-scale implications, *Sci. Mar.*, *65*(Supp. 2), 57–71, doi:10.3989/scimar.2001.65s257.
Kiørboe, T., C. Lundsgaard, M. Olesen, and J. L. S. Hansen (1994), Aggregation and sedimentation processes during a spring phytoplankton bloom: A field experiment to test coagulation theory, *J. Mar. Res.*, *52*(2), 297–323, doi:10.1357/0022240943077145.
Koeve, W., F. Pollehne, A. Oschlies, and B. Zeitzschel (2002), Storm-induced convective export of organic matter during spring in the northeast Atlantic Ocean, *Deep Sea Res., Part I*, *49*, 1431–1444, doi:10.1016/S0967-0637(02)00022-5.
Komar, P. D., A. P. Morse, L. F. Small, and S. W. Fowler (1981), An analysis of sinking rates of natural copepod and euphausiid faecal pellets, *Limnol. Oceanogr.*, *26*, 172–180, doi:10.4319/lo.1981.26.1.0172.
Körtzinger, A., U. Send, R. S. Lampitt, S. Hartman, D. W. R. Wallace, J. Karstensen, M. G. Villagarcia, O. Llinás, and M. D. DeGrandpre (2008), The seasonal pCO2 cycle at 49°N/16.5°W in the northeastern Atlantic Ocean and what it tells us about biological productivity, *J. Geophys. Res.*, *113*, C04020, doi:10.1029/2007JC004347.
Lampitt, R., B. Bett, K. Kiriakoulakis, E. Popova, O. Ragueneau, A. Vangriesheim, and G. Wolff (2001), Material supply to the abyssal seafloor in the Northeast Atlantic, *Prog. Oceanogr.*, *50*(1–4), 27–63, doi:10.1016/S0079-6611(01)00047-7.
Lampitt, R. S., I. Salter, B. A. de Cuevas, S. Hartman, K. E. Larkin, and C. A. Pebody (2010), Long-term variability of downward particle flux in the deep northeast Atlantic: Causes and trends, *Deep Sea Res., Part II*, *57*(15), 1346–1361, doi:10.1016/j.dsr2.2010.01.011.
Lee, C., S. G. Wakeham, and J. I. Hedges (2000), Composition and flux of particulate amino acids and chloropigments in equatorial Pacific seawater and sediments, *Deep Sea Res., Part I*, *47*(8), 1535–1568, doi:10.1016/S0967-0637(99)00116-8.
Lindemann, C., and M. A. St. John (2014), A seasonal diary of phytoplankton in the North Atlantic, *Frontiers Mar. Sci.*, *1*(37), 1−6, doi:10.3389/fmars.2014.00037.
Marshall, J., and F. Schott (1999), Open-ocean convection: Observations, theory, and models, *Rev. Geophys.*, *37*(1), 1–64, doi:10.1029/98RG02739.
Martin, J. H., G. A. Knauer, D. M. Karl, and W. W. Broenkow (1987), VERTEX: Carbon cycling in the northeast Pacific, *Deep Sea Res., Part I*, *34*(2), 267–285, doi:10.1016/0198-0149(87)90086-0.
Martin, P., R. S. Lampitt, M. Jane Perry, R. Sanders, C. Lee, and E. D'Asaro (2011), Export and mesopelagic particle flux during a North Atlantic spring diatom bloom, *Deep Sea Res., Part I*, *58*(4), 338–349, doi:10.1016/j.dsr.2011.01.006.
Mayor, D. J., R. Sanders, S. L. C. Giering, and T. R. Anderson (2014), Microbial gardening in the ocean's twilight zone: Detritivorous metazoans benefit from fragmenting, rather than ingesting, sinking detritus, *BioEssays*, *36*, 1132–1137, doi:10.1002/bies.201400100.
McDonnell, A. M. P., P. W. Boyd, and K. O. Buesseler (2015), Effects of sinking velocities and microbial respiration rates on the attenuation of particulate carbon fluxes through the mesopelagic zone, *Global Biogeochem. Cycles*, *29*, 175–193, doi:10.1002/2014GB004935.
Möller, K. O., M. St John, A. Temming, J. Floeter, A. F. Sell, J. P. Herrmann, and C. Möllmann (2012), Marine snow, zooplankton and thin layers: indications of a trophic link from small-scale sampling with the Video Plankton Recorder, *Mar. Ecol. Prog. Ser.*, *468*, 57–69, doi:10.3354/meps09984.
Moore, J. K., and T. A. Villareal (1996), Size-ascent rate relationships in positively buoyant marine diatoms, *Limnol. Oceanogr.*, *41*(7), 1514–1520, doi:10.4319/lo.1996.41.7.1514.
Morison, F., and S. Menden-Deuer (2015), Early spring phytoplankton dynamics in the subpolar North Atlantic: The influence of protistan herbivory, *Limnol. Oceanogr.*, *60*(4), 1298–1313, doi:10.1002/lno.10099.
Neuer, S., V. Ratmeyer, R. Davenport, G. Fischer, and G. Wefer (1997), Deep water particle flux in the Canary Island region: Seasonal trends in relation to long-term satellite derived pigment data and lateral sources, *Deep Sea Res., Part I*, *44*(8), 1451–1466, doi:10.1016/S0967-0637(97)00034-4.
Paulsen, M. L., K. Riisgaard, T. F. Thingstad, M. St John, and T. G. Nielsen (2015), Winter-spring transition in the subarctic Atlantic: Microbial response to deep mixing and pre-bloom production, *Aquat. Microb. Ecol.*, *76*(1), 49–69, doi:10.3354/ame01767.
Poulton, A. J., A. Charalampopoulou, J. R. Young, G. A. Tarran, M. I. Lucas, and G. D. Quartlya (2010), Coccolithophore dynamics in non-bloom conditions during late summer in the central Iceland Basin (July-August 2007), *Limnol. Oceanogr.*, *55*(4), 1601–1613, doi:10.4319/lo.2010.55.4.1601.
R Core Team (2015), R: A language and environment for statistical computing, R Found. for Stat. Comput., Vienna. [Available at http://www.R-project.org/.]
Raven, J. A., and A. M. Waite (2004), The evolution of silicification in diatoms: Inescapable sinking and sinking as escape?, *New Phytol.*, *162*(1), 45–61, doi:10.1111/j.1469-8137.2004.01022.x.
Riley, J. S., R. Sanders, C. Marsay, F. A. C. Le Moigne, E. P. Achterberg, and A. J. Poulton (2012), The relative contribution of fast and slow sinking particles to ocean carbon export, *Global Biogeochem. Cycles*, *26*(1), 1–10, doi:10.1029/2011GB004085.
Schindelin, J., et al. (2012), Fiji: An open-source platform for biological-image analysis, *Nat. Methods*, *9*(7), 676–682, doi:10.1038/nmeth.2019.
Sheridan, C., C. Lee, S. Wakeham, and J. K. Bishop (2002), Suspended particle organic composition and cycling in surface and midwaters of the equatorial Pacific Ocean, *Deep Sea Res., Part I*, *49*(11), 1983–2008, doi:10.1016/S0967-0637(02)00118-8.
Skreslet, S. (1988), Buoyancy in *Phaeocystis pouchetii* (Hariot) Lagerheim, *J. Exp. Mar. Biol. Ecol.*, *119*(2), 157–166, doi:10.1016/0022-0981(88)90230-4.
Smayda, T. (1970), The suspension and sinking of phytoplankton in the sea, *Oceanogr. Mar. Biol. Annu. Rev.*, *8*, 353–414.
Smetacek, V. (1985), Role of sinking in diatom life-history cycles: Ecological, evolutionary and geological significance, *Mar. Biol.*, *84*(3), 239–251, doi:10.1007/BF00392493.

Steinberg, D. K., C. A. Carlson, N. R. Bates, R. J. Johnson, A. F. Michaels, and A. H. Knap (2001), Overview of the US JGOFS Bermuda Atlantic Time-series Study (BATS): A decade-scale look at ocean biology and biogeochemistry, *Deep Sea Res., Part II*, *48*(8–9), 1405–1447, doi:10.1016/S0967-0645(00)00148-X.

Stemmann, L., G. A. Jackson, and D. Ianson (2004), A vertical model of particle size distributions and fluxes in the midwater column that includes biological and physical processes—Part I: Model formulation, *Deep Sea Res., Part I*, *51*(7), 865–884, doi:10.1016/j.dsr.2004.03.001.

Taylor, J. R., and R. Ferrari (2011), Shutdown of turbulent convection as a new criterion for the onset of spring phytoplankton blooms, *Limnol. Oceanogr.*, *56*(6), 2293–2307, doi:10.4319/lo.2011.56.6.2293.

Torres-Valdés, S., S. C. Painter, A. P. Martin, R. Sanders, and J. Felden (2014), Data compilation of fluxes of sedimenting material from sediment traps in the Atlantic Ocean, *Earth Syst. Sci. Data*, *6*(1), 123–145, doi:10.5194/essd-6-123-2014.

Townsend, D. W., M. D. Keller, M. E. Sieracki, and S. G. Ackleson (1992), Spring phytoplankton blooms in the absence of vertical water column stratification, *Nature*, *360*(6399), 59–62, doi:10.1038/360059a0.

Turner, J. T. (2002), Zooplankton fecal pellets, marine snow and sinking phytoplankton blooms, *Aquat. Microb. Ecol.*, *27*, 57–102, doi:10.3354/ame027057.

van Baalen, C., and R. M. Brown Jr. (1969), The ultrastructure of the marine blue green alga, *Trichodesmium erythraeum*, with special reference to the cell wall, gas vacuoles, and cylindrical bodies, *Arch. Mikrobiol.*, *69*(1), 79–91, doi:10.1007/BF00408566.

Van Ierland, E. T., and L. Peperzak (1984) Separation of marine seston and density determination of marine diatoms by density gradient centrifugation, *J. Plankton Res.*, *6*(1), 29–44, doi:10.1093/plankt/6.1.29.

Villa-Alfageme, M., F. C. de Soto, E. Ceballos, S. L. C. Giering, F. A. C. Le Moigne, S. Henson, J. L. Mas, and R. J. Sanders (2016), Geographical, seasonal and depth variation in sinking particle speeds in the North Atlantic, *Geophys. Res. Lett.*, *43*, doi:10.1002/2016GL069233.

Villareal, T. A. (1988), Positive buoyancy in the oceanic diatom *Rhizosolenia debyana* H. Peragallo, *Deep Sea Res., Part A*, *35*(6), 1037–1045, doi:10.1016/0198-0149(88)90075-1.

Villareal, T. A., C. H. Pilskaln, J. P. Montoya, and M. Dennett (2014), Upward nitrate transport by phytoplankton in oceanic waters: Balancing nutrient budgets in oligotrophic seas, *PeerJ*, *2*, e302, doi:10.7717/peerj.302.

Waite, A., and P. Harrison (1992), Role of Sinking and ascent during sexual reproduction in the marine diatom *Ditylum-Brightwellii*, *Mar. Ecol. Prog. Ser.*, *87*, 113–112.

Walsby, A. E. (1978), The properties and buoyancy-providing role of gas vacuoles in Trichodesmium Ehrenberg, *Br. Phycol. J.*, *13*(2), 103–116, doi:10.1080/00071617800650121.

Woods, S., and T. Villareal (2008), Intracellular ion concentrations and cell sap density in positively buoyant oceanic phytoplankton, *Nov. HEDWIGIA Suppl.*, *113*, 131–145.